Additive manufacturing of flexible thermoplastic polyurethane (TPU): enhancing the material elongation through process optimisation

Progress in Additive Manufacturing
https://doi.org/10.1007/s40964-024-00790-y

FULL RESEARCH ARTICLE

Additive manufacturing of flexible thermoplastic polyurethane (TPU): enhancing the material elongation through process optimisation

Viccica Marco[1] · Giordano Massimo[1] · Galati Manuela[1]

Received: 5 October 2023 / Accepted: 28 August 2024

Abstract
Thermoplastic polyurethane (TPU) is used to produce elastomeric parts with superior wear/abrasion resistance, toughness, shock absorption properties, and flexibility, even at low temperatures. The production of this material through additive manufacturing (AM) techniques has been increasing because of the possibility of tuning the mechanical properties using structural design and build process parameters. Despite the data being limited, TPU produced by AM, mainly based on material extrusion, is much stiffer than the corresponding produced by conventional manufacturing, and, therefore, it shows a limited elongation. This study presents the mechanical characterization of TPU produced by the infrared light powder bed fusion (PBF-IrL) system (HP multi-jet fusion), which has recently been introduced. The properties are compared with TPU produced by open (3ntrA4) and closed (Markforged) material extrusion (MEX) systems. For the open FDM, the effects of the processing conditions are investigated to improve the material elongation and UTS with respect to the data reported in the literature for AM and conventional manufacturing. For this reason, an extensive and comprehensive review has been carried out. Compared to material extrusion, PBF-IrL TPU specimens showed higher Young's modulus, but poorer A%. Considering the samples produced by MEX and compared to previous results in the literature, the properties obtained in this study are superior both in terms of UTS and A%.

Keywords Thermoplastic polyurethane · Additive manufacturing · Fused deposition modeling · Multi jet fusion · Elongation at break · TPU

1 Introduction

The countless opportunities that additive manufacturing (AM) technologies provide in research and industry have accelerated the demands in optimizing materials for specific applications. In this regard, polymeric materials have received particular attention. Among them, over the last few years, one of the most explored polymeric materials is polyurethane thermoplastic (TPU). The high elasticity and biocompatibility, combined with the possibility of having complex shapes by AM processes, have fascinated many sectors of applications, such as footwear [1], medical devices [2], wearables electronics [3], energy absorbers [4], and textiles [5]. Since the chemical composition of TPU is based on a succession of soft and hard copolymer segments (polyols and diisocyanates) [6], the properties of elastomers and thermoplastics are combined by balancing elasticity and strength. The chemical content variation of soft and hard segments permits various grades of TPU, typically recognized by the hardness level and measured by the Shore A and D values. Also, TPU is characterized by good abrasion and tear resistance, flexibility at low temperatures, and biodegradability [7]. The TPU softness provides a remarkable adhesion with some other polymeric materials, enabling the manufacture of multi-material components. When produced via AM, these object based on TPU allow mechanical and multi-functional properties that meet specific demands [8].

To tune the mechanical properties, TPU is also considered in composite parts consisting of a TPU matrix material and a reinforcement material, such as carbon nanotube (CNT) [9], boron nitride nanosheets (BNN) [10], graphene [11], hybrid hexagonal boron nitride (h-BN) [12], and thermoplastic such as PLA [13].

✉ Galati Manuela
manuela.galati@polito.it

[1] Integrated Additive Manufacturing Center (IAM), Department of Management and Production Engineering, Politecnico di Torino, Turin, Italy

Published online: 10 September 2024

A further strategy for the properties adjustment of TPU-made parts is strictly related to the main advantage of AM technology, the freedom of designing complex geometries. Some studies have investigated TPU cellular structure geometry, such as lattice, TPMS, and honeycomb [14].

Currently, TPU is mainly processed by material extrusion AM processes, most commonly identified as fused deposition modeling (FDM). The reasons are the easy use of the machine and the low-cost process. Nevertheless, the production via FDM has some limitations regarding dimension, geometrical complexity and the need for support structures. Because of that, some industrial AM machine manufacturers introduced the use of support material removable by chemical operation [15].

In contrast, polymer powder bed AM processes can be an alternative solution for greater design freedom. In these cases, also complex parts can be produced without using support structures [16–18]. The main processes are PBF laser beam (PBF-LB or selective laser sintering, SLS) or infrared lamp (PBF-IfL or multi-jet fusion, MJF). However, little knowledge of processing TPU using such technology is present in the literature. This can be explained by the fact that TPU powder has been only recently commercialized by SLS and MJF machines and powders suppliers. So far, preliminary results showed that TPU produced by the PBF techniques is more brittle than its FDM counterparts [19].

On the other hand, FDM-made TPUs have been deeper analyzed. Literature is thoroughly disseminated of works that attempt to optimize process parameters to enhance the quality of TPU artifacts in terms of surface, geometrical and mechanical qualities. Most studies have determined that nozzle temperature (NT) and layer thickness (LT) are the main parameters influencing TPU strength [20]. Further investigations highlighted the relevance of determining a proper range of NT, when combined with the drying process, to decrease or remove moisture from TPU filaments [21]. In contrast, C. Hohimer et al. [22] asserted that NT is less significant when it is analyzed in combination with the path (or raster) orientation and the air gap parameters (distance between two adjacent filaments, which can be changed by varying the hatch distance). Therefore, a negative air gap value should avoid internal porosities. In addition, owing to the low viscosity of TPU, attention must be paid to the feeding ratio and infill speed parameters that, if correctly set, can avoid under-extrusion and stringing problems [23].

Even if a considerable effort was made to optimize several process parameters, up to date, the mechanical properties are acceptable for some applications but are still not comparable to the values of flexibility and strength achieved through traditional manufacturing techniques such as injection molding (IM) [24]. The reason is intrinsically connected to the FDM process, in which the component is made of layers of bonded filaments. The strength of the bonding depends on many combined conditions, e.g., layer thickness, extrusion temperature, raster or path orientation, print speed, build orientation, number of walls, and hatch distance [25]. For a specific TPU material with the same hardness value, there is no evidence of parameters window that can provide higher or comparable mechanical properties than the conventional injection molded counterparts.

In comparison to their conventional counterparts, the current work seeks to identify and optimize the mechanical characteristics window of TPU components made using various AM processes. In light of the literature findings, a process optimization study has been performed using a design of experiment (DoE) approach, which has been executed on a desktop FDM printer. In this regard, the interaction between layer thickness, infill speed, and hatch distance was selected as factors for the DoE because it has never been investigated in the literature. For each combination of process parameters, tensile test samples were printed and tested in three replicas. The results were analyzed statistically.

Further comparisons were made by testing two novel TPU materials recently released on the market and still not mechanically analyzed in the literature. The above-cited materials are characterized by the same hardness and processed via different AM technology: Fused Filament Fabrication (FFF) by Markforged® and MJF by HP®.

The quality of the printed material was evaluated regarding the deposition strategy, porosity, and internal defects via microscope and computed tomography X-ray scans.

The mechanical properties were compared with data from the literature for additive and conventional manufacturing technologies.

2 Materials and methods

In this study, TPU flat dumbbell-shaped test specimens were produced using different AM systems. The production methods for polymeric materials with AM technologies depend on the feedstock material, powder (PBF processes), or filament (MEX processes).

The HP® JetFusion 4200 MultiJetFusion is a PB-IrL/P system. This technology features the ESTANE® 3D TPU M95A-545 as powder feedstock material.

The Markforged MarkTwo system is a FFF [26] equipment (0.4 mm nozzle diameter), and the related material is named Smooth TPU 95A filament (1.75 mm diameter).

The 3ntr A4v3 is a FDM technology device (0.4 mm nozzle diameter) equipped for this investigation with Elasto85A filament (2.85 mm diameter).

FDM and FFF are MEX processes in which the polymer is bonded by thermal reaction (MEX-TRB/P/TPU).

Beyond the technology, it is worth noticing that each machine adopts different software for job preparation. In

particular, the HP MultiJetFusion system and the Markforged MarkTwo use closed-parameters slicers in which only a few settings can be modified, whereas the 3ntr A4v3 features an open slicer modification of all the process parameters. To a fair comparison, the specimens printed by HP MultiJetFusion and MarkTwo were produced with the optimal parameters indicated by the machine suppliers, whereas the DoE was performed on the A4v3. In the second step, according to the limit of the slicer, an additional set of specimens was produced for comparison, as reported in Sect. 2.2 and Sect. 2.3.

2.1 Design and production with HP MultiJetFusion

For the HP JetFusion 4200 MJF system, the flat dumbbell-shaped test specimens design followed the BS EN ISO 527–2:2012, as depicted in Fig. 1.

A packing density of 2.2% and an irradiance of −2% were selected. The layer thickness was set to 100 µm. The ESTANE® 3D TPU M95A powder used for the production is recycled 80%, meaning that 20% of the powder of the production batch was virgin. TPU powder size ranges between 20 and 250 µm with a D_v (50) of 85.2 µm [27]. The preheating temperature for the printing process is maintained nearing to 106 °C, the onset melting temperature of the TPU powder [27]. After production, specimens were cooled in air, and the excess powder was cleaned with glass microspheres with a diameter of 300 µm in a blasting device at 6 bars.

Owing to the powder-based nature of the technology, the samples were produced with different orientations to evaluate how thermal shrinkage and building direction affect mechanical properties [28]. The build volume was saturated with several specimens differently oriented with respect to the build direction: flat (F), edge (E), and vertical (V), as depicted in Fig. 2.

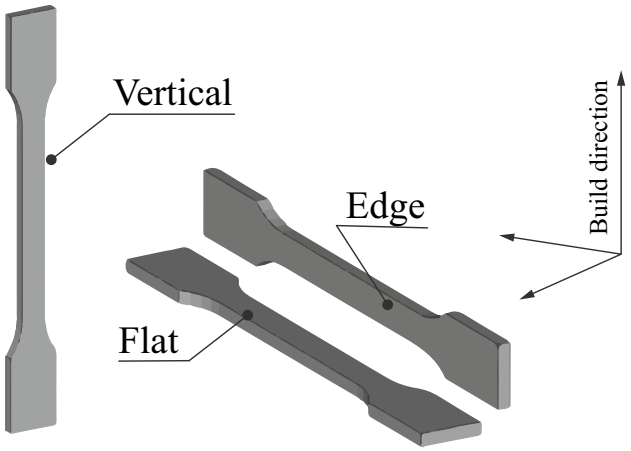

Fig. 2 Specimens' orientation in the HP JetFusion 4200

2.2 Design and production with Markforged technology

The specimens for the Markforged MarkTwo system were designed according to EN ISO/ASTM D638 – Type IV (Fig. 3).

As mentioned above, the slicer software, Eiger™, limits the process parameter setting to the layer thickness, fill pattern and density, roof and floor layers, and wall layers. In particular, the roof and the floor layers are material layers printed automatically with a contour offset strategy and an infill density equal to 100%.

For the current study, a preliminary set of specimens were manufactured with the standard set of parameters (MF standard in Table 1). This set involves the use of a triangular fill pattern with a corresponding infill density equal to 37% (Fig. 4a). To increase the infill density and make it worth the comparison with the other specimens, a second set of specimens was fabricated, constraining the software to obtain an infill density equal to 100% (MF case 2 in Table 1), at least in the gage length. Since the triangular infill allows only a maximum infill density equal to 55%, the number of roof and floor was increased to the maximum and equal to 10 (Fig. 4b). In addition, to obtain a full density, at least in the gage length, in the remaining layers also, the number of

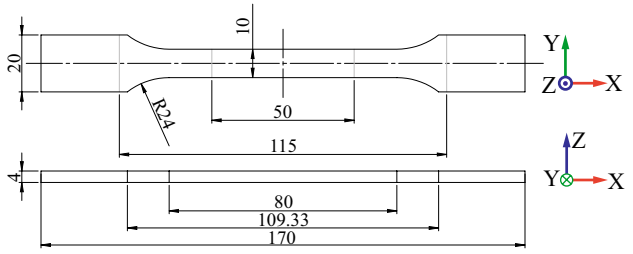

Fig. 1 Dumbbell-shaped specimens corresponding to BS EN ISO 527–2:2012 (dimensions in mm)

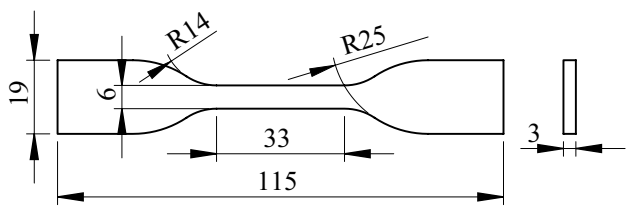

Fig. 3 Dumbbell shape specimen following the EN ISO/ASTM D638–Type IV (dimensions in mm)

Table 1 Process parameters on Eiger™ for the D638 dumbbell specimens produced with Markforged MarkTwo

Parameter	MF standard	MF case 2
Layer thickness [mm]	0.1	0.1
Fill density (floor and roof layers)	100%	100%
Fill density (intermediate layers)	37%	55%
Fill direction	45°	45°
Fill pattern	Triangular	Triangular
Number of roofs and floor	6	10
Number of wall layers	2	15
Hatch distance [mm]	0.4	0.4

Table 2 Process parameters on KISSlicer for the D638 dumbbell specimens produced with 3ntr A4v3

Parameter	A4v3 standard	A4v3 case 2
Layer thickness [mm]	0.2	0.2
Fill direction	45°	45°
Fill pattern	Straight	Rounded
Fill density (top 6 layers and bottom 6 layers)	100%	100%
Fill density (intermediate layers)	100%	33.3%
Hatch distance [mm]	0.3	0.4
Extrusion temperature [°C]	220	220
Platform temperature [°C]	110	110
Infill speed [mm/s]	20	30

walls was increased to maximum and equal to 15 (Fig. 4b). Table 1 summarizes the process parameters and in Fig. 4 shows the path of the deposited material for the configurations mentioned above.

2.3 Design and production with FDM open-source system

For the 3ntr A4v3, the specimens were designed according to EN ISO/ASTM D638 – Type IV (Fig. 3). The associated slicer is KISSlicer©, an open-source slicer that fully manages the process parameters.

Initially, a set of specimens was printed using the printing parameters suggested by the machine supplier for TPU (Set A4v3 standard in Table 2).

For comparison purposes, an additional set of specimens was printed with a lower infill density to emulate the specimens printed by MarkTwo using the MF standard (A4v3 case 2 in Table 2).

Figure 5 highlights the differences in the infill pattern.

An optimization of the process parameters was then performed through a DoE approach. The factors under analysis were the layer thickness (3 levels), the hatch distance (2 levels), the infill speed (2 levels), and their effect on the material elongation. The designed plan consisted of 12 combinations of parameters: LT was varied with three levels equal to 0.15 mm, 0.20 mm and 0.25 mm, respectively; HD which was selected as 0.3 mm and 0.4 mm; and the infill speed (IS) which was chosen equal to 20 mm/s and 30 mm/s. Each set of parameters was identified with a numerical index (ID) in Table 3.

Three replicas were printed for each parameter set and tested under tensile load. Therefore, considering the additional preliminary sets of specimens, globally, 42 specimens were produced and investigated.

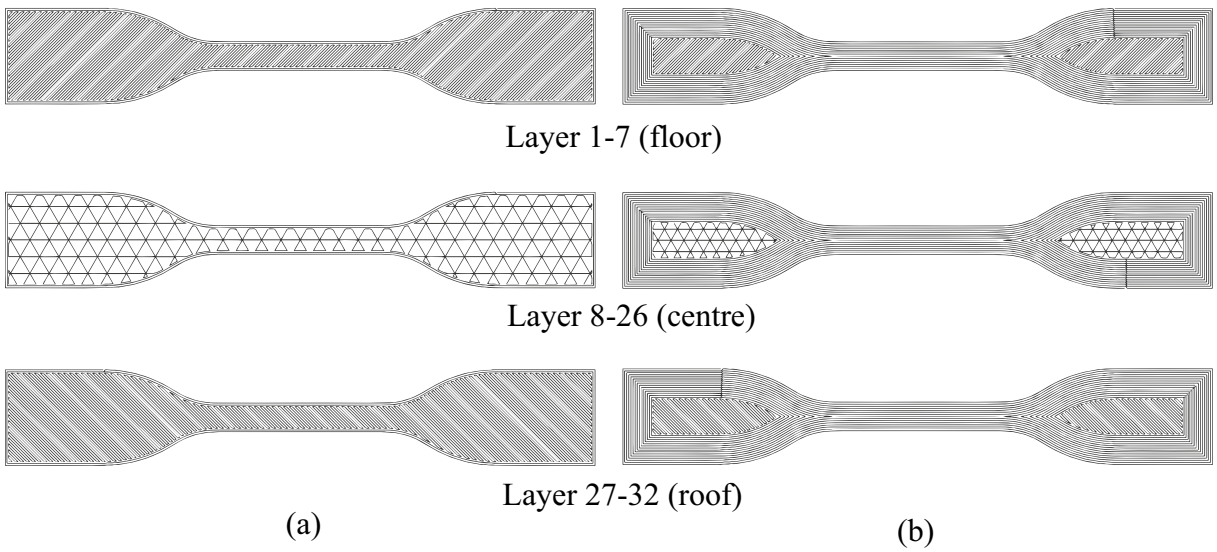

Fig. 4 D638 dumbbell shape specimens for **a** Markforged standard process parameters; **b** modified process parameters

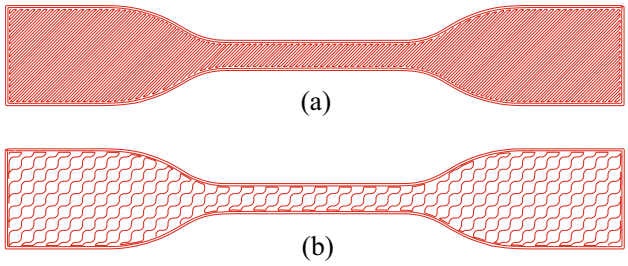

Fig. 5 KISSlicer slicing previews of the D638 dumbbell specimen **a** A4v3 standard and **b** A4v3 case 2

Table 3 Process parameters in 12 different combinations

ID	Layer thickness [mm]	Hatch distance [mm]	Infill speed [mm/s]
1	0.15	0.4	20
2	0.15	0.3	30
3	0.20	0.3	20
4	0.15	0.4	30
5	0.20	0.4	20
6	0.25	0.4	20
7	0.25	0.4	30
8	0.15	0.3	20
9	0.20	0.3	30
10	0.25	0.3	30
11	0.20	0.4	30
12	0.25	0.3	20

All the samples were laid on a substrate or High Impact PolyStyrene to avoid the stitching of the specimen on the printing plate and to prevent undesired elongation during part removal. The support material was deposited from a different extruder.

2.4 Geometrical and mechanical characterizations

Single deposited tracks of material were analyzed using an optical microscope (i.e., Leica S9i) to evaluate the actual width of the deposited track.

The fracture surface after the tensile test was analyzed using an optical microscope (i.e., Leica DM6 M) to correlate the process parameters, mechanical properties, and geometrical quality of the section.

X-ray computed tomography (CT scan GE Phoenix v|tome|x s) scanning was executed on one replica of each printed sample. The scan settings are 80 kV, 200 µA current for 1001 projections resulting in a 17.5 µm voxel size. The scanned volume corresponded to the gage length of the sample, e.g., the volume was of around $40 \times 10 \times 4$ mm^3 for the HP samples. The 3D volume reconstruction and the subsequent analyses have been performed using VGStudio Max 3.4. The tomograms were used to evaluate and compare the processes in terms of internal defects and porosity.

Uniaxial tensile tests have been carried out on an AURA 10 T | Easydur Italiana equipment with 10 kN of maximum capacity. The strain rate was constant during the test and equal to 50 mm/min was imposed up to sample failure. The load/displacement output data, collected with a 50 Hz sampling frequency, were converted into stress–strain curves. Following the prescriptions of ASTM D638-22, the stress–strain graphs were adjusted by compensating the initial part of the curve, i.e., redefining the zero cross on the strain axis. Raw data from the tensile tests were processed in MATLAB®. Young's modulus (E), Ultimate Tensile Strength (UTS), and Elongation at break (A%) were calculated. Young's modulus (E) is computed dividing the stress (σ) by the strain (ε) (Eq. 1). The stress (Eq. 2) was obtained dividing the force (F) by the initial undeformed section (A_0).

$$E = \frac{\sigma}{\varepsilon} \tag{1}$$

$$\sigma = \frac{F}{A_0} \tag{2}$$

The cross-sectional dimension, A_0, was measured within the calibrated length with a 0.01 mm precision micrometer considering the average of three sections measured at the center of the sample and the end point. The value was obtained as the average of three measurements.

The strain was calculated as reported in Eq. 3, where Δl is the crosshead displacement, and l_0 represents the starting gage length.

$$\varepsilon = \frac{\Delta l}{l_0} \tag{3}$$

UTS and A% are extracted as the maximum value of stress and the maximum value in strain percentage, respectively.

3 Results

The average tensile test curve for each set of manufactured replicas according to DoE is reported in Fig. 6. The standard deviation generated by the tested replicas was reported for the stress at different values of the strain: 20%, 100%, 300%, 600%, and 900% in Fig. 6 and Table 4. Analogously, the deviation for the strain at given stress is reported for the stress of 10 MPa, 20 MPa, and UTS in Table 4.

Figure 7 shows the calculated mechanical properties. The height of the bar represents the average value of the characteristic over the three replicas, while the segment

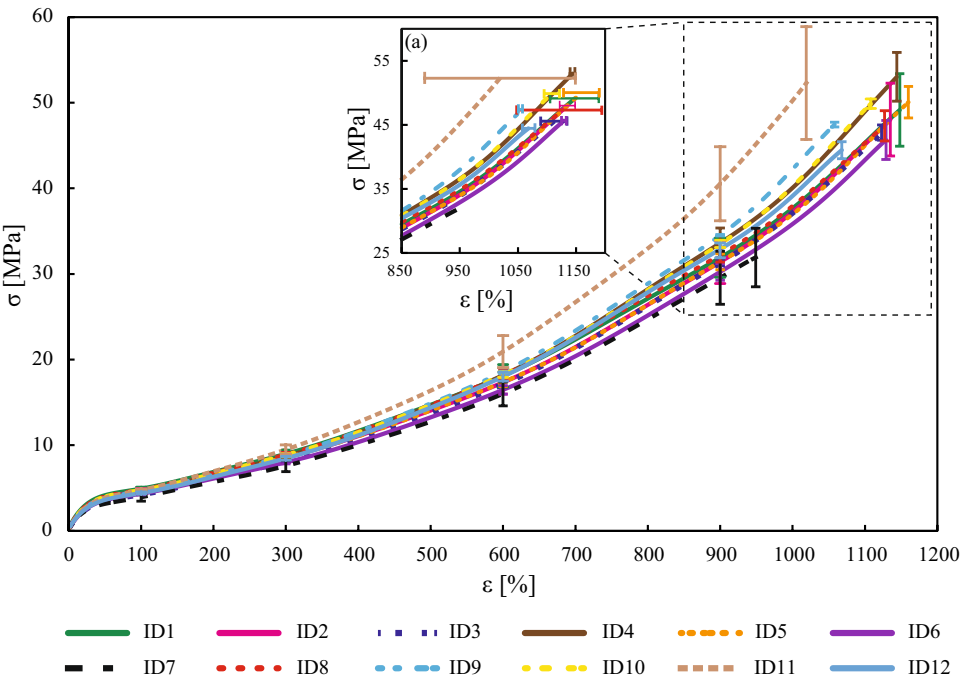

Fig. 6 Stress vs strain graph of Elasto85A samples manufactured with twelve different configurations of process parameters. The deviations of the mean stress are reported measured at the strain of 20%, 600%, and the break point. The window **a** reports the deviation of the strain at the break point

Table 4 Data referring to Fig. 6. Mean and standard deviation (SD) values of stress at different strain percentages and strain at different stress values

	Mean (SD)								
	Stress at the strain of						Strain at the stress of		
	20%	100%	300%	600%	900%	*A%	10 MPa	20 MPa	*UTS MPa
ID	[MPa]						[%]		
1	2.8 (0.1)	4.9 (0.2)	9.0 (0.4)	18.1 (1.3)	31.9 (2.3)	49.1 (4.2)	350 (6.1)	881 (11.5)	1044 (14.4)
2	2.5 (0.2)	4.6 (0.3)	8.6 (0.6)	17.3 (1.4)	31.4 (2.5)	48.0 (4.2)	372 (8.9)	900 (7.8)	1154 (6.4)
3	2.3 (0.1)	4.3 (0.1)	8.1 (0.1)	17.1 (0.3)	31.3 (0.3)	46.5 (0.9)	373 (7.1)	872 (6.4)	1124 (11)
4	2.4 (0.1)	4.6 (0.1)	8.7 (0.3)	18.2 (0.8)	33.6 (1.7)	53.0 (2.8)	358 (6.2)	847 (2.1)	1029 (3.6)
5	2.5 (0.1)	4.7 (0.1)	8.6 (0.3)	17.4 (0.5)	31.4 (0.9)	50.1 (1.8)	359 (12.6)	870 (17.5)	1142 (20.8)
6	2.3 (0.1)	4.3 (0.1)	8.0 (0.2)	16.5 (0.5)	30.2 (1.0)	45.7 (2.3)	385 (11.1)	894 (19.6)	1098 (26.1)
7	2.1 (0.3)	3.9 (0.5)	7.6 (0.7)	16.0 (1.4)	29.5 (3.1)	31.9 (3.4)	402 (35)	/	879 (64.7)
8	2.6 (0.1)	4.8 (0.1)	8.9 (0.2)	18.2 (0.6)	32.2 (0.9)	47.3 (1.8)	349 (16)	865 (23.1)	1077 (34.4)
9	2.5 (0.1)	4.6 (0.1)	8.8 (0.1)	18.6 (0.1)	34.5 (0.1)	47.4 (0.3)	344 (4.2)	819 (0.8)	1055 (1.7)
10	2.6 (0.1)	4.8 (0.1)	8.9 (0.1)	18.2 (0.3)	33.5 (0.4)	49.9 (0.6)	344 (6.2)	833 (8.2)	1101 (6.3)
11	2.5 (0.1)	4.8 (0.1)	9.5 (0.5)	20.9 (1.9)	40.5 (4.3)	52.3 (6.6)	317 (21.3)	753 (45.5)	1070 (65.4)
12	2.3 (0.1)	4.4 (0.1)	8.5 (0.2)	18.0 (0.5)	32.7 (0.9)	44.5 (1.0)	359 (10.4)	840 (15.5)	1081 (11.9)

*values at the break consistent with the mean curves reported in Fig. 6

represents the standard deviation of the measure. Those data are grouped according to the process parameters. The detailed data referring to Fig. 7 are reported in Appendix in Table A1.

As shown in Fig. 6, the maximum elongation is over 1100% for most of the tested parameters. The sets of parameters that showed the lower A% corresponded to the ones with the highest UTS. For instance, sample ID11, which was manufactured with IS of 30 mm/s, HD of 0.4 mm, and LT of 0.2 mm, shows the highest mean value with the lowest deviation of UTS (57.6 ± 0.4 MPa) among all configurations. However, observing A%, the sample ID11 shows the highest standard deviation (i.e., 1073 ± 70%). That means that the reliability of this process parameters set is low because the elongation is the more critical property of elastomers and is unstable. In this regard, samples with a LT 0.15 mm

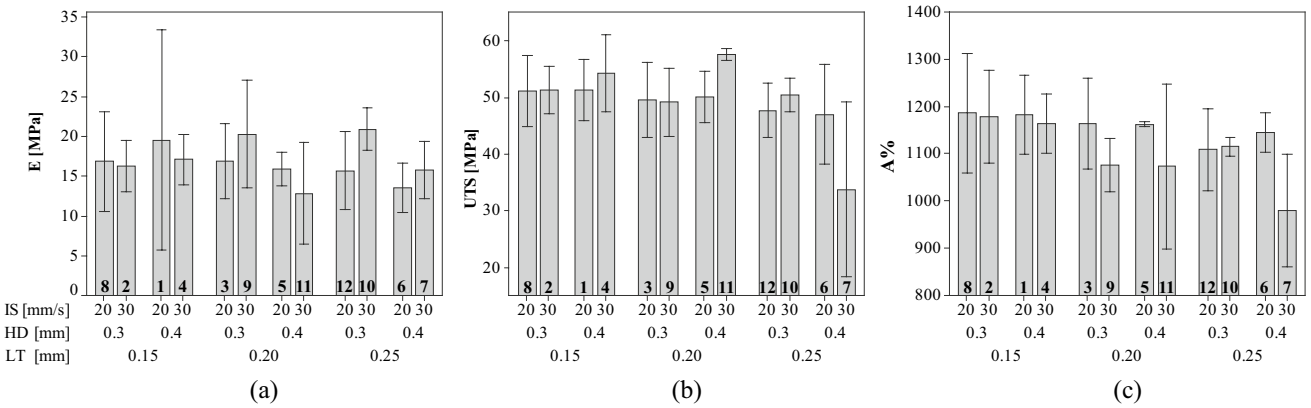

Fig. 7 Bar plot of **a** E, **b** UTS, and **c** A% mean and standard deviation against the analyzed process parameters: infill speed (IS), hatch distance (HD), and layer thickness (LT)

exhibited a superior A% mean value. Therefore, it is evident that the process parameters significantly affected the mechanical response in terms of UTS and A%.

The elastic region is limited at an extremely low strain percentage, and the curves overlap in that range. The limited elastic zone makes the evaluation of E difficult, and because of that, in some cases, the dispersion of the results is large (Fig. 7a). The process parameters do not significantly affect the mechanical property.

In agreement with Ref. [20] and as observed above, the layer thickness significantly affects the strength of the FDM artifacts. The lower the layer height, the higher the UTS response (Fig. 8a). This behavior may be caused mainly by the presence of interlayer porosity, which decreases the bond strength, as shown in the tomography image of Fig. 12. Indeed, as observed by Rajpurohit and Dave [29], higher LT values are usually laid with lower feed pressure, which generates less interlayer adhesion due to the reduced bonding area. In contrast, the hatch distance and infill speed values appeared to be less significant on UTS in the range of the investigated parameters. Since the hatch distance parameter represents the distance of the centerline of two adjacent tracks deposited, its dimension is directly related to the overlapping and air gap phenomena. In addition, during the G-code generation, KISSlicer tunes the internal feeding parameters to correctly deposit the material based on the HD and LT set. Consequently, even if the HD remains constant, the actual raster width dimension may change with the LT height, as schematically illustrated in Fig. 9. Hence, the minimum overlapping can be guaranteed for low values of LT combined with the HD of 0.3 mm and 0.4 mm (see Fig. 9). These findings are confirmed by the analysis performed on

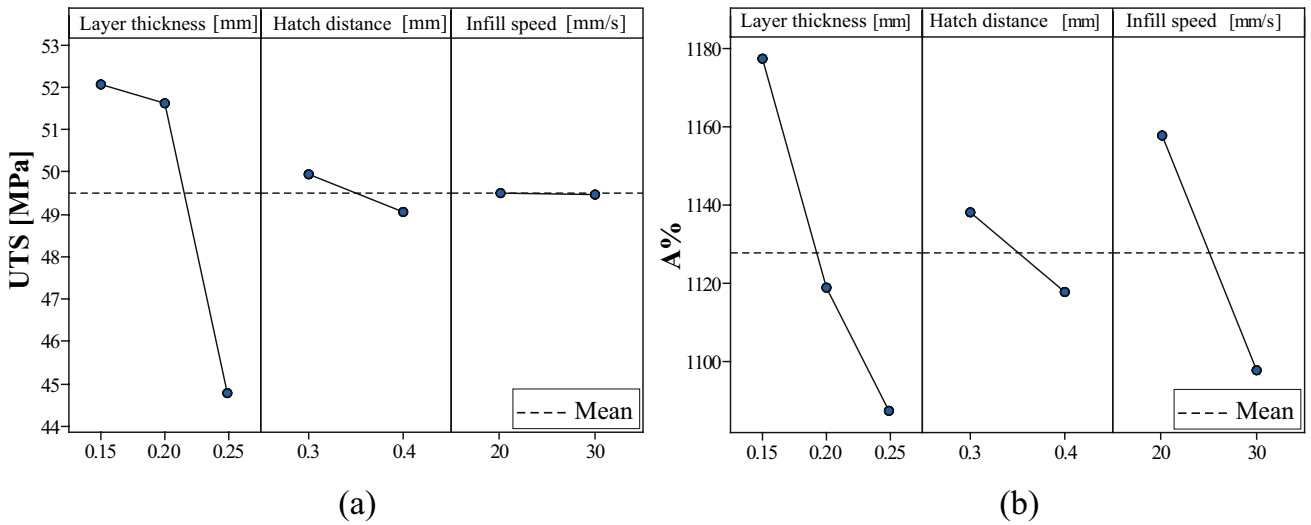

Fig. 8 Main effects plot of **a** UTS and **b** A% against the analyzed process parameters

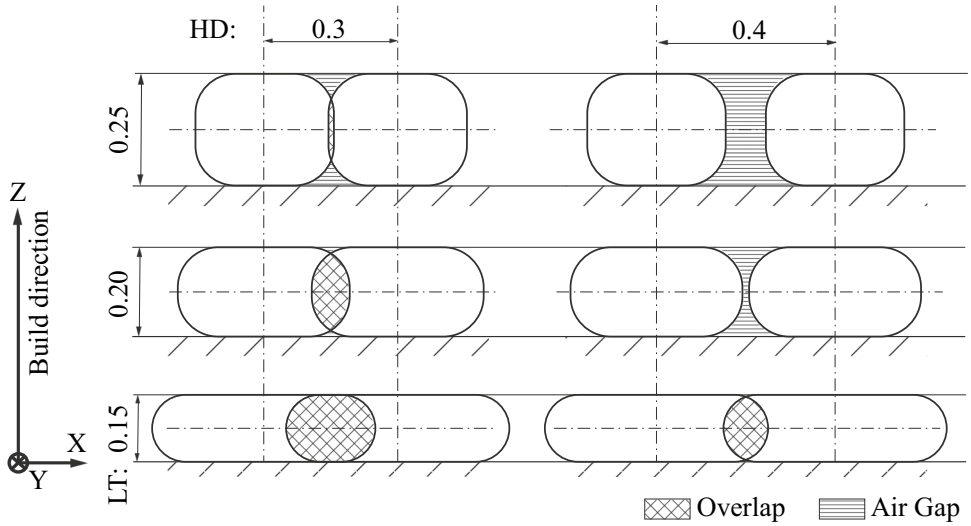

Fig. 9 Air gap and overlap variation of two adjacent filaments with LT and HD (dimensions in mm)

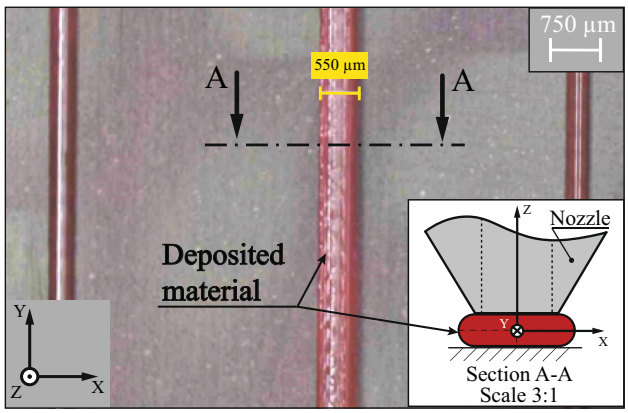

Fig. 10 Single track to evaluate the raster width with respect to the nominal value of HD and LT settings (LT = 0.15 mm, HD = 0.4 mm)

the optical microscope shown in Fig. 10. The single track deposited with LT = 0.15 mm and HD = 0.4 mm shows an actual raster width dimension greater than the diameter of the nozzle (0.4 mm), i.e., 0.55 mm.

In addition, despite the main effect of the IF on the UTS is not averagely significant (Fig. 8a), its contribution to the strength variation of samples manufactured with high LT is meaningful.

Most influential are the parameters for the Elongation at break. Each increase of all the process parameters corresponds to a decrease in the A% (Fig. 8b). The higher interlayer bonding observed with decreasing the LT parameter allows the samples to get a high strain percentage with a more accentuated trend than the UTS results. Moreover, the IS and HD influence on the A% is more significant than the UTS response. The higher percentage of filaments overlapping (HD = 0.3 mm) results in a late generation and propagation of the internal cracks up to the failure. The fewer the internal gaps, the more the bonding among the filaments withstand the tensile load. Also, the raster direction at ± 45° leads the stress to spread across the perpendicular cross section. At the same time, a slow filament deposition is ideal for consolidating the filaments' bonds along each layer, generating fewer internal defects.

In light of the findings reported above, the coefficient of variation (CV) was calculated as an index for comparing the different parameters set and highlighting the best result in terms of A% considering the mean (μ) and the standard deviation (SD) values. CV is an index of the repeatability of the assay and, since it is independent of measurement units, provides a good metric to compare different mechanical properties [30]. CV is calculated as shown in Eq. 4.

$$CV = \frac{SD}{\mu} \tag{4}$$

Low CV values (high mean and low SD values) mean a robust process and therefore are preferable. Therefore, the best configuration is represented by the parameters set that shows the lowest CV. The CV values for each configuration are reported in Fig. 11. As can be observed and as discussed above, sample ID11 shows an extremely poor CV in terms of A%, while samples ID10 and ID5 represent the optimal compromise between UTS and A%. However, as mentioned before, the main advantage of this material is represented by its exceptional elongation property. Therefore, it can be established that the best process parameters are corresponding to sample ID 5 (0.20 mm of layer thickness, 0.40 mm of hatch distance, and 20 mm/s of infill speed).

These conclusions are consistent with the qualitative porosity measured with CT scan analyze, reported in Fig. 12. From a physical perspective, the same flow rate

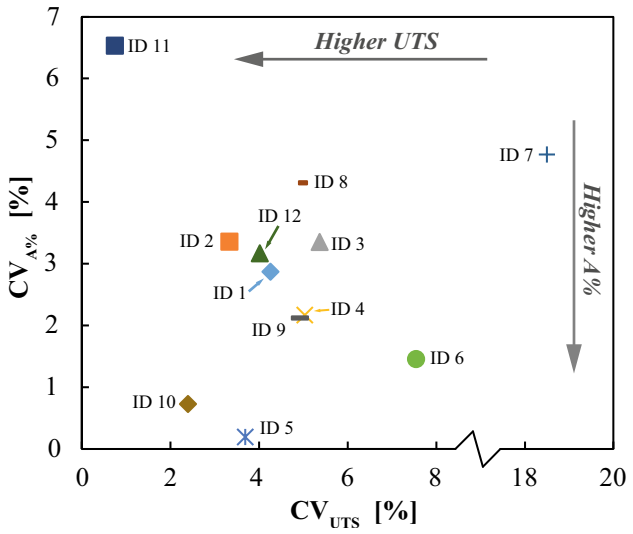

Fig. 11 Scatter plot of CV calculated for UTS and A% across the DoE samples

of material leads to a lower pressure for increased layer thickness and infill speed; thus, the bonding between layers is generally weaker. The ID7 (Fig. 12b) sample has higher layer thickness and infill speed than ID5 (Fig. 12a). Combining those process parameters determines the adhesion quality between the layers and between the infill and external walls. The increased parameters of specimen ID7 (Fig. 12b) lead to a generally worse adhesion, resulting in higher porosity and poorer mechanical properties (see Table 4).

Similar conclusions can be drawn by observing the fracture surface of the same samples. ID 5 (Fig. 13a) presents the deposited tracks compacted and overlapped. ID7 specimens (Fig. 13b) present a fracture surface where the air gaps between the tracks might justify the lower resistance.

The best result selected from the 3ntrA4 (Elasto 85A with 100% of density) is compared with results from the specimens produced using the Markforged system (Smooth TP 95A with 100% and 37% of density) and specimen produced to emulate the standard printing conditions of Markforged (Elasto 85A with 33% of density) (Fig. 14). The trends of the mechanical properties differ significantly. The UTS values of the samples printed with MarkTwo are almost double those of the corresponding samples printed with 3ntrA4. On the contrary, A% is much lower. This result can be explained by considering the Shore hardness of the material. The Markforged filament has a higher Shore hardness (95A) than the filament used for printing the specimen by 3ntrA4, which leads to higher material stiffness, while A% decreases [31].

Even if the strength at the break of the stiffer TPU (i.e., 95A) is double compared to the stress at the same strain of the other, the UTS of the latter is much higher with double A%. This behavior is identically scaled down to the specimens with lower fill density. The mechanical properties are not proportional to the fill density. The fully dense sample break occurs at higher UTS (about 50%) and higher A% (20–40%) than the specimens with the lower density.

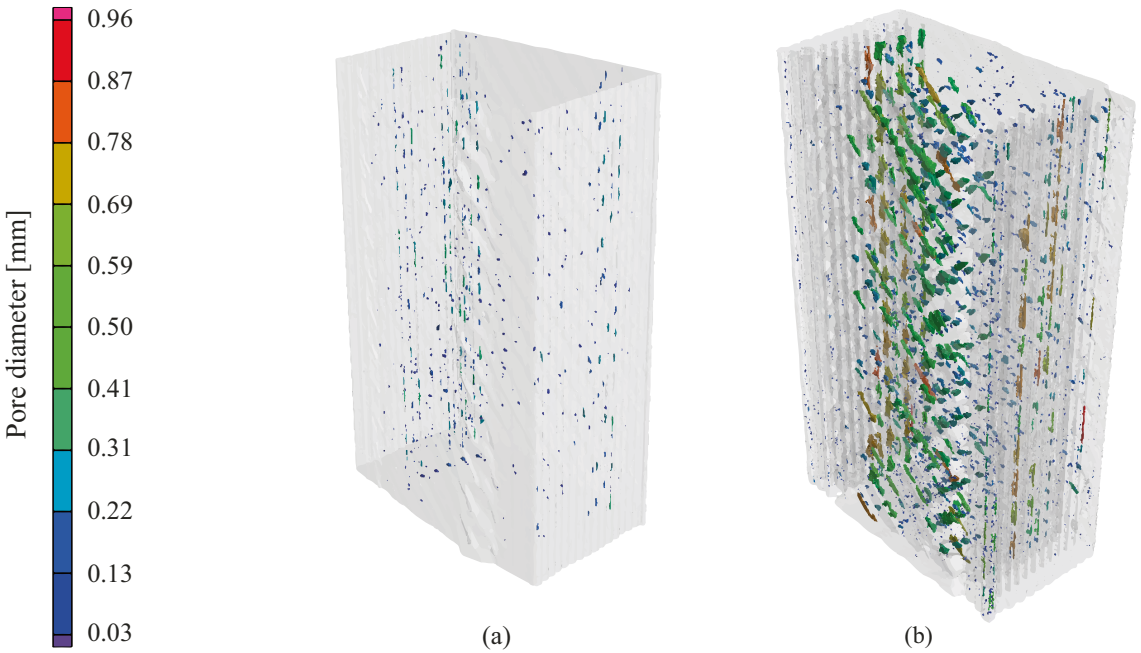

Fig. 12 Qualitative porosity of the 3ntr produced specimens **a** ID 5 and **b** ID 7

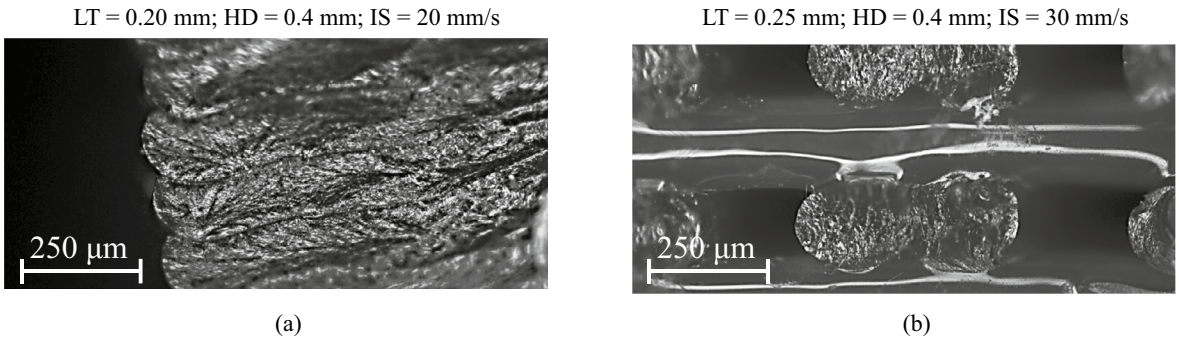

Fig. 13 Fracture surface of the 3ntr produced specimens **a** ID 5 and **b** ID 7

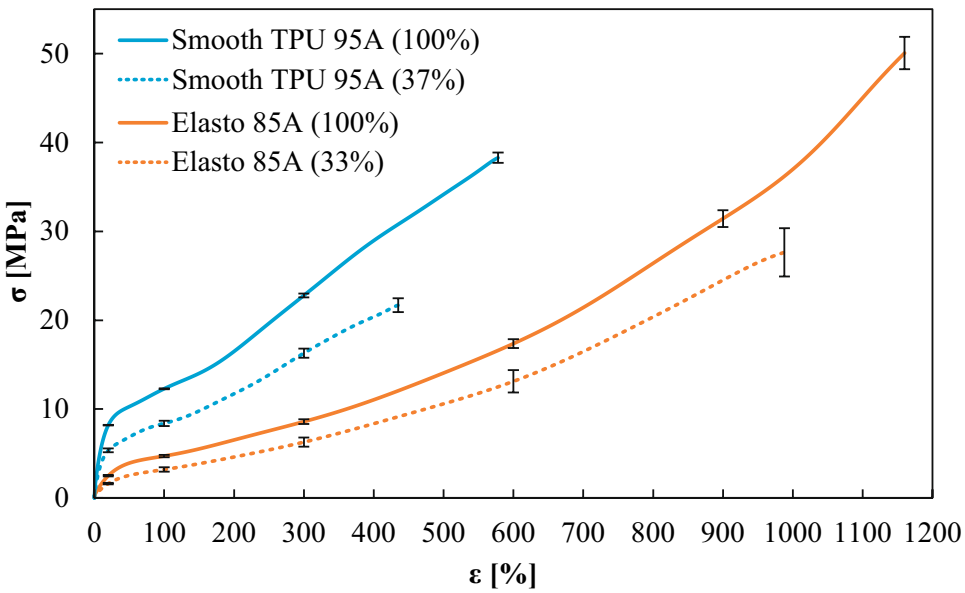

Fig. 14 Stress vs strain graph of Smooth TPU 95A and Elasto85A specimens manufactured with full dense and reduced infill

The stress and strain curves for the Estane TPU M95A-545 manufactured via MJF and the different building orientations are reported in Fig. 15.

The build orientation influences the tensile properties significantly. Vertical specimen has the poorest properties due to the layer-by-layer strategy, for which the vertically oriented specimens present numerous little sections compared to the flatted and edged ones, which are manufactured with fewer and wider sections. Also, the internal porosities of powder-based parts generate a brittle behavior in this material, as confirmed in Ref [32]. Therefore, owing to the weak connection between the layers, applying a tensile load to the vertical dumbbell samples causes cracks diffusion and the increment of delamination phenomena.

These findings are also supported by the CT scan analysis as depicted in Fig. 16. The flat orientation (Fig. 16c) has a generally distributed porosity with a more evident defects accumulation close to the external surface. The edge orientation (Fig. 16b) results in the lowest porosity level

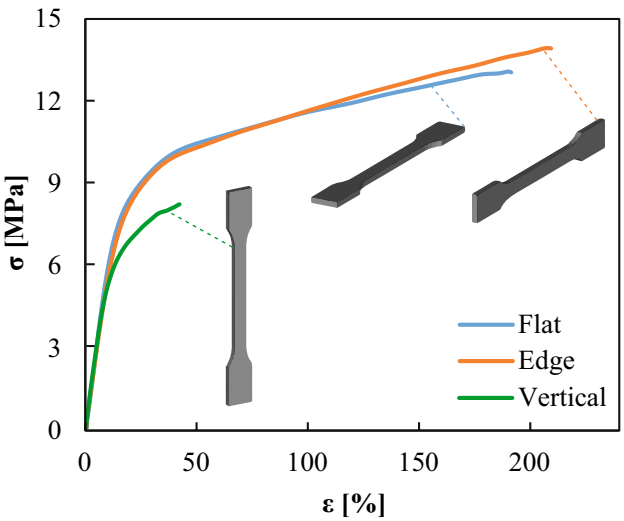

Fig. 15 Stress vs strain graph of the Estane TPU M95A-545 manufactured in flat, edge, and vertical orientations via MJF

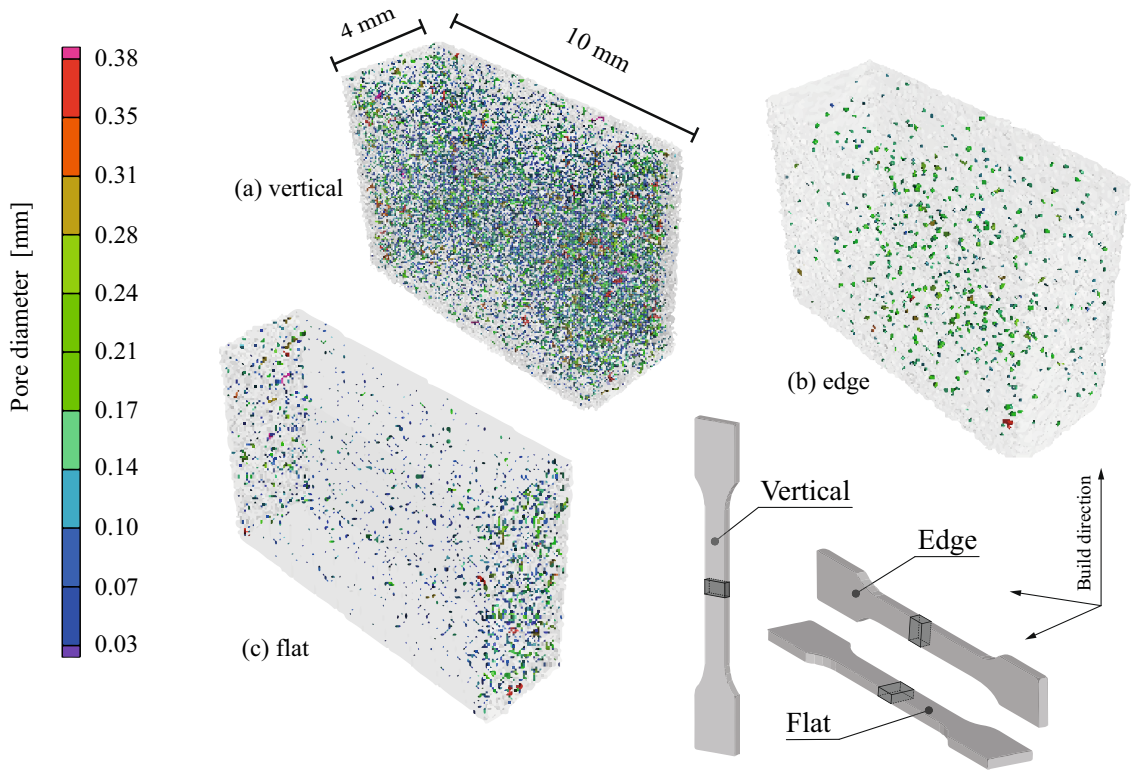

Fig. 16 Qualitative porosity of a portion ($10\times4\times8 mm^3$) of Estane TPU M95A-545 specimens calibrated zone manufactured in flat (**a**), edge (**b**), and vertical (**c**) orientations

homogeneously distributed in the calibrated section but with a slightly more prominent dimension of the defects. Instead, the vertical orientation (Fig. 16a) has a severe cloud of porosities, and the defects are generally larger than the other building orientations. The observed distribution is typical of PBF for polymers processes (e.g., Ref [28].). Therefore, the jetting of the section in the longitudinal direction, namely in the load direction, leads to a more resistant coupon. The building orientation defines the porosity level and reflects mechanical resistance.

Figure 17 resumes all the data presented this work. Overall, the differences in the materials and AM processes are significant. Although the TPU parts produced by Mark-Two and MJF technologies have the same hardness grade,

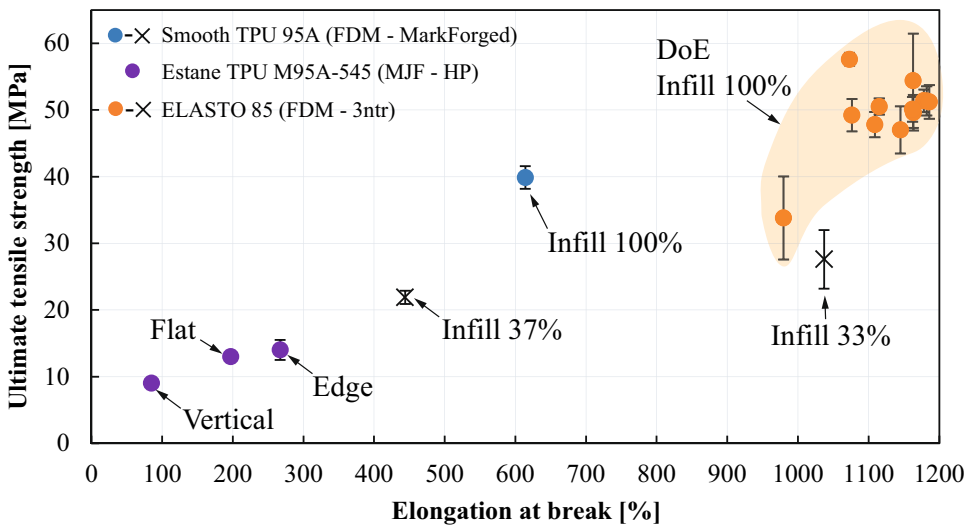

Fig. 17 Comparison of UTS versus A% graph for FDM and MJF specimens manufactured and tested in this work

significantly different strength and elastic behavior were observed. Generally, the FDM specimen showed superior mechanical performance.

The obtained data are compared with several TPUs optimized for production via the AM technologies (SLS, MJF, FDM) and a more conventional manufacturing, injection molding. Since the primary index of subdivision of elastomeric materials is the Shore hardness, the data has been grouped according to the Shore A/D scale [33] and identified as Medium Hard, Hard, and Extra Hard. A summary is reported as Shore A/D versus UTS and A% in Fig. 18 and Fig. 19, respectively. The values referring to graphs in Fig. 18 and Fig. 19 were extracted from Ref. [34].

As can be observed, a large variety of hardness grades have been tested in the literature.

Among the AM technologies, as already pointed out in the graph of Fig. 17, extruded TPU materials (FDM) are superior in terms of UTS compared to SLS and MJF. Fixing the hardness grade, in most cases, TPU processed by IM guarantee better values of UTS (Fig. 18) than the AM counterparts among most of the hardness values analyzed. The values obtained in this work are superior among the AM processed materials and performed better than the counterpart obtained by IM process. This finding is also valid for A% (Fig. 19), for which exceptional values were detected compared to other technologies and previous results regarding FDM production.

4 Conclusion

This work investigated the mechanical properties of TPU produced by different additive manufacturing technologies and tested under tensile load. The technologies included are a closed FDM system (Markforged), a PBF-IrL/P system (HP), and an open FDM machine (3ntrA4). In particular, the FDM process has been optimized to obtain comparable mechanical performance concerning parts produced by injection molding. The optimization has been performed using a DoE approach in which the layer thickness (LT), the hatch distance (HD), and the infill speed (IS) have been varied.

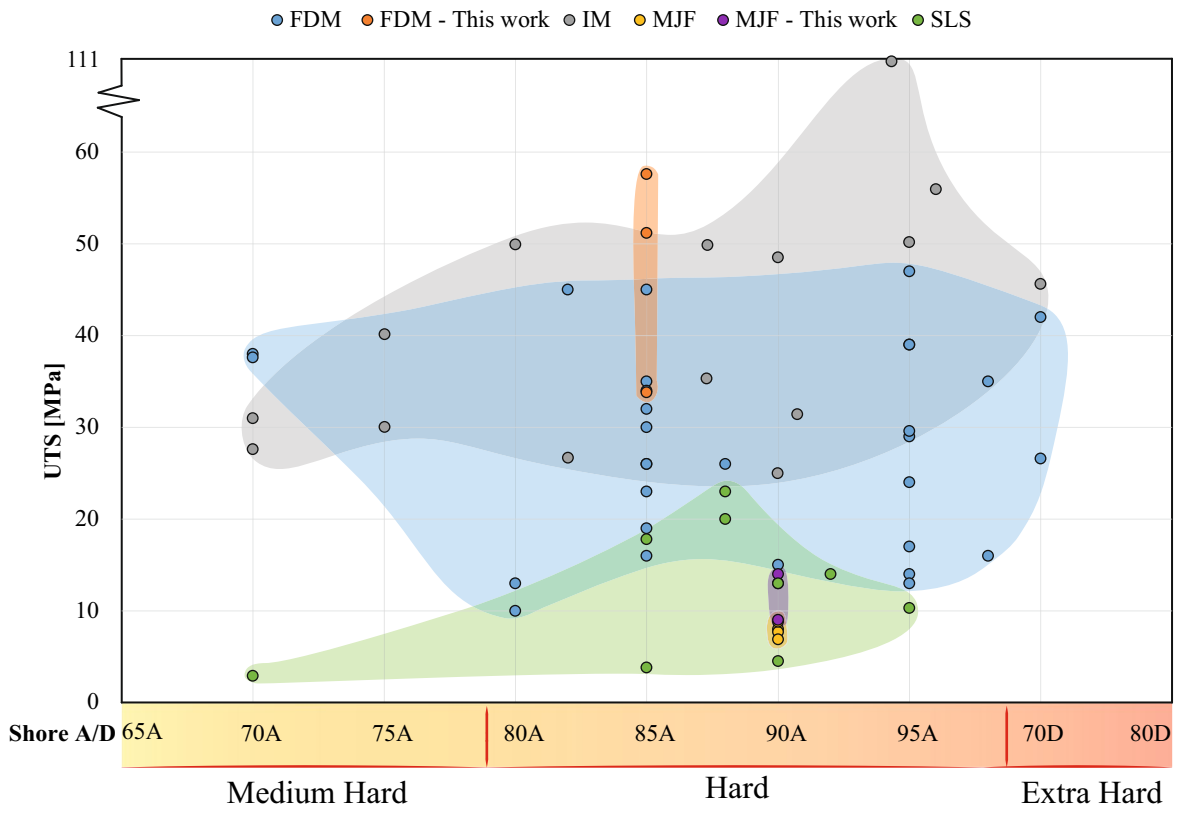

Fig. 18 UTS versus Shore A/D hardness of different grades of TPU materials manufactured with the main additive manufacturing technologies (FDM, MJF, SLS) and Injection Molding (IM) traditional process compared with the materials analyzed in the present study

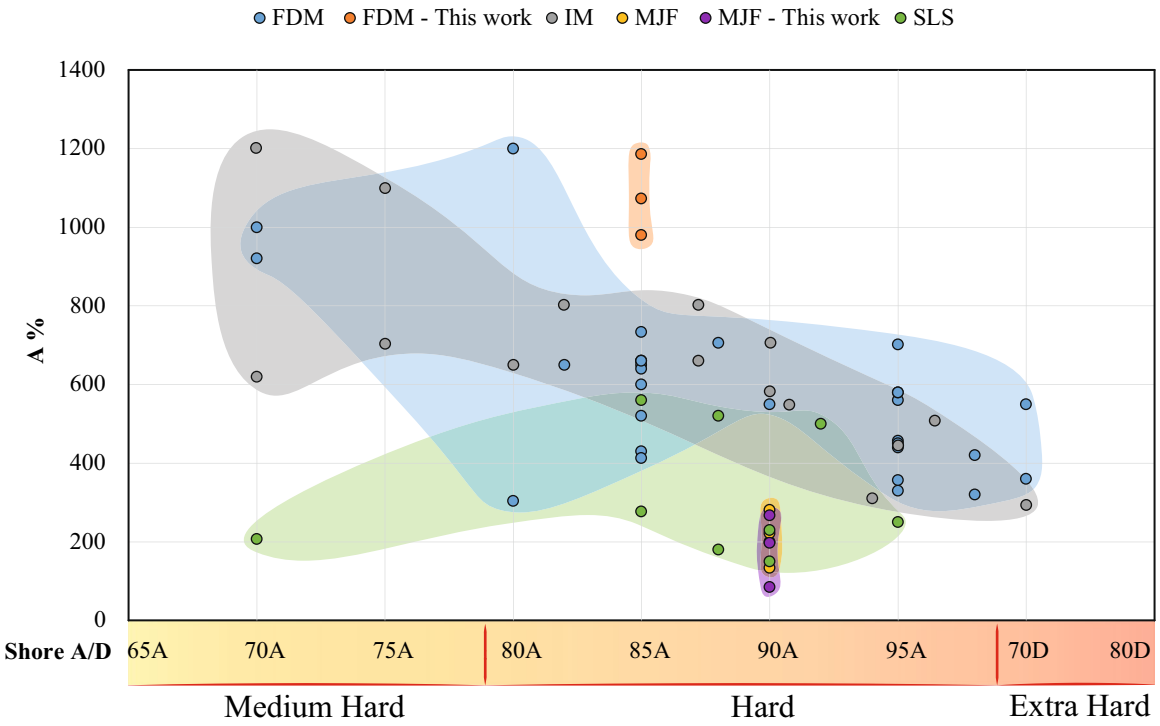

Fig. 19 A% versus Shore A/D hardness of different grades of TPU materials manufactured with the main additive manufacturing technologies (FDM, MJF, SLS) and Injection Molding (IM) traditional process compared with the materials analyzed in the present study

The experimental investigation showed that layer thickness is the parameter that mainly affected the mechanical properties with the highest values of A% with 0.15 mm of LT. The best combination of parameters that exhibits the highest repeatability of the results and a significant value of elongation (A% = 1162 ± 2% and a UTS = 50 ± 1.8 MPa) is represented by ID5 obtained with LT = 0.20 mm, HD = 0.40 mm, and IS = 20 mm/s. Overall, the investigated parameters have shown a physical and mechanical interdependence between each other that, if correctly set, allows obtaining high fully dense TPU parts capable of reaching outstanding A% with excellent tensile strength.

Due to the difference in shore A hardness, the Markforged TPU (95A) shows higher strength at low strain. However, the TPU processed with the 3ntr system (85A) can reach a UTS value up to 20% higher and a much higher A%.

Compared to FDM specimens, MJF (PBF-IrL/P) TPU specimens showed higher Young's modulus, but poorer A%. Therefore, despite the greater design freedom allowed by a PBF process, the poorest Elongation at break may hinder the application of such process for certain application, such as spiral hoses and hydraulic seals. However, to the best of the authors' knowledge, the mechanical characterization reported in this study represents, up to date, the first results available TPU powder for MJF.

Compared to previous results in the literature, including conventional injection molding, the properties obtained in this study are superior both in terms of UTS and A%. The optimized process for TPU led to about 45% higher Elongation at break than the IM counterparts and even superior mechanical results compared to other additive manufacturing techniques.

This work has contributed to investigating the appealing mechanical properties of the TPU manufactured via different additive manufacturing technologies, with a focus on the process parameters optimization of an FDM machine. Also, the conducted review of the mechanical properties of commercial TPU materials could guide engineers to better design artifacts by choosing the best solutions regarding the material hardness and AM process.

Appendix

See Table A1

Table A1 Mean and SD values of the ultimate tensile strength (UTS), elongation at break, and Young's modulus (E) evaluated among all the replicas of the DoE

Mean (SD)			
ID	UTS [MPa]	A [%]	E [MPa]
1	51.3 (2.2)	1182 (34)	19.6 (5.6)
2	51.4 (1.7)	1178 (40)	16.2 (1.3)
3	49.6 (2.7)	1163 (39)	16.9 (1.9)
4	54.4 (2.7)	1163 (25)	17.1 (1.3)
5	50.1 (1.8)	1162 (2)	15.9 (0.9)
6	47.0 (3.5)	1145 (17)	13.6 (1.2)
7	33.8 (6.2)	980 (48)	15.8 (1.4)
8	51.2 (2.5)	1186 (51)	16.9 (2.5)
9	49.2 (2.4)	1076 (23)	20.3 (2.7)
10	50.5 (1.2)	1115 (8)	20.9 (1.1)
11	57.6 (0.4)	1073 (70)	12.9 (2.6)
12	47.8 (1.9)	1109 (35)	15.7 (2.0)

Acknowledgements The authors acknowledge Dr. Marco Macchi from Maralbi srl, Via dal Bosc 25/e, Romans d'Isonzo (GO) for providing the sample produced by the HP® JetFusion 4200 MultiJetFusion system and Dr. Alessandro Barraco and Giuseppe Trovato from 3D COMPANY srl, Via Bellardi 36/A, Torino for providing the samples produced by the Markforged MarkTwo system.

Funding Open access funding provided by Politecnico di Torino within the CRUI-CARE Agreement. No organization provided funding to the authors for the work they submitted. There are no material financial or non-financial interests to disclose.

Data availability The authors confirm that the data supporting the findings of this study are available within the article and are openly available in Ref. [34].

Declarations

Conflict of interest The authors did not receive support from any organization for the submitted work. The authors have no relevant financial or non-financial interests to disclose.

References

1. Claybrook FR, Mohammed M, Southee DJ (2022) Investigation of additive manufactured Split P TPMS elastomeric structures for diabetic foot insoles. Trans Addit Manuf Meets Med 4:1–4
2. Xiao J, Gao Y (2017) The manufacture of 3D printing of medical grade TPU. Prog Addit Manuf 2:117–123. https://doi.org/10.1007/s40964-017-0023-1
3. Niu C, Luan C, Shen H et al (2022) Tunable soft–stiff hybridized fiber-reinforced thermoplastic composites using controllable multimaterial additive manufacturing technology. Addit Manuf 55:102836. https://doi.org/10.1016/j.addma.2022.102836
4. Anni IA, Uddin KZ, Pagliocca N et al (2022) Out-of-plane load-bearing and mechanical energy absorption properties of flexible density-graded TPU honeycombs. Compos Part C Open Access 8:100284. https://doi.org/10.1016/j.jcomc.2022.100284
5. Kabir S, Kim H, Lee S (2020) Physical property of 3D-printed sinusoidal pattern using shape memory TPU filament. Text Res J 90:2399–2410. https://doi.org/10.1177/0040517520919750
6. Gumus OY, Ilhan R, Canli BE (2022) Effect of printing temperature on mechanical and viscoelastic properties of ultra-flexible thermoplastic polyurethane in material extrusion additive manufacturing. J Mater Eng Perform 31:3679–3687. https://doi.org/10.1007/s11665-021-06510-9
7. Jayswal A, Adanur S (2022) An overview of additive manufacturing methods, materials, and applications for flexible structures. J Ind Text 52:152808372211146. https://doi.org/10.1177/15280837221114638
8. Żur A, Żur P, Michalski P, Baier A (2022) Preliminary study on mechanical aspects of 3D-printed PLA-TPU composites. Materials (Basel) 15:1–15. https://doi.org/10.3390/ma15072364
9. Li Z, Wang Z, Gan X et al (2017) Selective laser sintering 3D printing: a way to construct 3D electrically conductive segregated network in polymer matrix. Macromol Mater Eng 302:1–10. https://doi.org/10.1002/mame.201700211
10. Gao J, Hao M, Wang Y et al (2022) 3D printing boron nitride nanosheets filled thermoplastic polyurethane composites with enhanced mechanical and thermal conductive properties. Addit Manuf 56:102897. https://doi.org/10.1016/j.addma.2022.102897
11. Maldonado MP, Pinto GM, Costa LC, Fechine GJM (2022) Enhanced thermally conductive TPU/graphene filaments for 3D printing produced by melt compounding. J Appl Polym Sci. https://doi.org/10.1002/app.52405
12. Jiang Y, Li J, Leng J, Zhang J (2022) Extrusion-based additive manufacturing samples with desirable thermal conductivities prepared by incorporating hybrid hexagonal boron nitride(h-BN) and novel process strategy. Macromol Mater Eng 307:1–9. https://doi.org/10.1002/mame.202100715
13. Rahmatabadi D, Ghasemi I, Baniassadi M et al (2022) 3D printing of PLA-TPU with different component ratios: fracture toughness, mechanical properties, and morphology. J Mater Res Technol 21:3970–3981. https://doi.org/10.1016/j.jmrt.2022.11.024
14. Viccica M, Galati M, Calignano F, Iuliano L (2022) Design, additive manufacturing, and characterisation of a three-dimensional cross-based fractal structure for shock absorption. Thin-Walled Struct 181:110106
15. Kumar A, Verma S, Jeng JY (2020) Supportless lattice structures for energy absorption fabricated by fused deposition modeling. 3D Print Addit Manuf 7:85–96. https://doi.org/10.1089/3dp.2019.0089
16. Tewani H, Hinaus M, Talukdar M, et al (2022) Architected syntactic foams: a tale of additive manufacturing and reinforcement parameters

17. Yuan S, Shen F, Bai J et al (2017) 3D soft auxetic lattice structures fabricated by selective laser sintering: TPU powder evaluation and process optimization. Mater Des 120:317–327. https://doi.org/10.1016/j.matdes.2017.01.098
18. Heiml E, Hössinger-Kalteis A, Major Z (2022) Experimental characterization of 3D printed cellular structures. Mater Today Proc 62:2528–2532. https://doi.org/10.1016/j.matpr.2022.03.124
19. Dadbakhsh S, Verbelen L, Vandeputte T et al (2016) Effect of powder size and shape on the SLS processability and mechanical properties of a TPU elastomer. Phys Procedia 83:971–980. https://doi.org/10.1016/j.phpro.2016.08.102
20. Lin X, Coates P, Hebda M et al (2020) Experimental analysis of the tensile property of FFF-printed elastomers. Polym Test 90:106687. https://doi.org/10.1016/j.polymertesting.2020.106687
21. Bruère VM, Lion A, Holtmannspötter J, Johlitz M (2022) Under-extrusion challenges for elastic filaments: the influence of moisture on additive manufacturing. Prog Addit Manuf 7:445–452. https://doi.org/10.1007/s40964-022-00300-y
22. Hohimer C, Christ J, Aliheidari N et al (2017) 3D printed thermoplastic polyurethane with isotropic material properties. Behav Mech Multifunct Mater Compos 10165:1016511. https://doi.org/10.1117/12.2259810
23. Lin X, Gao J, Wang J et al (2021) Desktop printing of 3D thermoplastic polyurethane parts with enhanced mechanical performance using filaments with varying stiffness. Addit Manuf 47:102267. https://doi.org/10.1016/j.addma.2021.102267
24. Xiang N, Zhang X, Zheng M et al (2021) Investigation of tensile behavior and molecular structure of the thermoplastic polyurethane sheets injection molded at different mold temperatures. J Appl Polym Sci 138:1–15. https://doi.org/10.1002/app.50959
25. Dey A, Yodo N (2019) A systematic survey of FDM process parameter optimization and their influence on part characteristics. J Manuf Mater Process. https://doi.org/10.3390/jmmp3030064
26. Galati M, Viccica M, Minetola P (2021) A finite element approach for the prediction of the mechanical behaviour of layered composites produced by continuous filament fabrication (CFF). Polym Test. https://doi.org/10.1016/j.polymertesting.2021.107181
27. Tey WS, Cai C, Zhou K (2021) A comprehensive investigation on 3d printing of polyamide 11 and thermoplastic polyurethane via multi jet fusion. Polymers (Basel). https://doi.org/10.3390/polym13132139
28. Calignano F, Giuffrida F, Galati M (2021) Effect of the build orientation on the mechanical performance of polymeric parts produced by multi jet fusion and selective laser sintering. J Manuf Process 65:271–282. https://doi.org/10.1016/j.jmapro.2021.03.018
29. Rajpurohit SR, Dave HK (2018) Effect of process parameters on tensile strength of FDM printed PLA part. Rapid Prototyp J 24:1317–1324. https://doi.org/10.1108/RPJ-06-2017-0134
30. Huang DJ, Li H (2021) A machine learning guided investigation of quality repeatability in metal laser powder bed fusion additive manufacturing. Mater Des 203:109606. https://doi.org/10.1016/j.matdes.2021.109606
31. Materials EI, Manufacturing CB, Hardness D, Laboratories C (2010) Standard Test Method for Rubber Property—Durometer Hardness 1 This standard is for EDUCATIONAL USE ONLY. 5:1–13. https://doi.org/10.1520/D2240-15R21.2.
32. Galati M, Calignano F, Defanti S, Denti L (2020) Disclosing the build-up mechanisms of multi jet fusion: experimental insight into the characteristics of starting materials and finished parts. J Manuf Process 57:244–253. https://doi.org/10.1016/j.jmapro.2020.06.029
33. Qi HJ, Joyce K, Boyce MC (2003) Durometer hardness and the stress-strain behavior of elastomeric materials. Rubber Chem Technol 76:419–435. https://doi.org/10.5254/1.3547752
34. Viccica M, Galati M, Giordano M (2023) Literature database in mechanical characteristic of Thermoplastic Polyurethane